

# Determining the index of refraction of polar stratospheric clouds above Andoya (69°N) by combining size-resolved concentration and optical scattering measurements

Terry Deshler,<sup>1</sup> Bruno Nardi,<sup>1,2</sup> Alberto Adriani,<sup>3</sup> Francesco Cairo,<sup>3</sup> Georg Hansen,<sup>4</sup> Federico Fierli,<sup>5</sup> Alain Hauchecorne,<sup>5</sup> and Lucio Pulvirenti<sup>3</sup>

**Abstract.** Observations within two polar stratospheric clouds (PSCs) of aerosol scattering and size-resolved aerosol concentration were compared to infer the index of refraction of the PSC particles. The observations were completed in situ with balloon-borne aerosol counters and a laser scatterometer (692, 830 nm) and remotely with an ozone (308, 353 nm) and Rayleigh (532, 1064 nm) lidar. A Monte Carlo analysis, accounting for the errors of the individual measurements, indicates the comparison method has a precision of  $\pm 0.03$  for an index of refraction range of 1.30–1.60. Measurements from all instruments were obtained in one PSC with relatively little vertical or horizontal structure. The comparison suggested that the index of refraction of the PSC particles was near  $1.47 \pm 0.01$  in the nondepolarizing region of the cloud and  $1.52\text{--}1.56 \pm 0.04$  in the depolarizing region. These values were consistent for the observations at 308, 353, 692, and 830 nm. The comparisons with the Rayleigh lidar were not as consistent. Aerosol volumes inferred from the particle measurements agree closely with volumes expected for liquid ternary aerosol (LTA) at the base of the cloud, with nitric acid trihydrate (NAT) above 23 km, in the depolarizing region, and with both LTA and NAT in the bulk of the nondepolarizing portion of the cloud. A much more limited set of measurements was obtained in a second PSC with strong vertical structure, evident in the temperature and aerosol profiles. Comparisons in this cloud were difficult because of the inherent problems in comparing in situ and remote measurements in clouds with strong vertical and horizontal structure. In this PSC the comparisons of in situ aerosol size distribution and remote aerosol scattering did not converge to a clear index of refraction.

## 1. Introduction

During polar night, stratospheric air can radiatively cool to temperatures below the condensation points of nitric acid and water, resulting in polar stratospheric clouds (PSCs). On these cloud particles, heterogeneous reactions involving HCl and ClONO<sub>2</sub> rapidly produce photolabile chlorine compounds, ensuring that as the polar stratosphere is exposed to sunlight, halogens can catalytically destroy ozone. The PSCs also facilitate the catalytic halogen cycles through the removal of reactive nitrogen from the polar stratosphere.

Knowledge of the size, number, chemical composition, and physical state of PSC particles is important to assess the magnitude of ozone depletion, because of the dependence of heterogeneous reaction rates on the amount of aerosol surface available and on the character of the particle surface [Ravishankara and Hanson, 1996]. Laboratory and theoretical studies have suggested several possibilities for the composition

of PSC particles above the ice point: nitric acid trihydrate (NAT) [Crutzen and Arnold, 1986; Toon et al., 1986; Hanson and Mauersberger, 1988], nitric acid dihydrate (NAD) [Worsnop et al., 1993], and liquid ternary aerosol (LTA) [Arnold, 1992; Carslaw et al., 1994; Tabazadeh et al., 1994]. There are many observations of PSCs above the ice frost point [e.g. Fahey et al., 1989; Hofmann and Deshler, 1991; Dye et al., 1992], and direct measurements of nitric acid within PSC particles [Pueschel et al., 1989, 1990]; however, field measurements of exact PSC composition are only beginning [Schreiner et al., 1999]. Observations in both hemispheres point to the existence of both liquid droplets and solid hydrates within PSCs [Dye et al., 1992; Adriani et al., 1995; Dye et al., 1996; Del Negro et al., 1997], while thermodynamic considerations indicate that liquid and solid particles can coexist in equilibrium over a wide range of conditions [Koop et al., 1997b].

In the lower stratosphere, there is an abundance of aqueous H<sub>2</sub>SO<sub>4</sub> (sulfate) aerosol that serves as nuclei for PSC particles. Although laboratory studies show that upon cooling sulfuric acid droplets can form sulfuric acid tetrahydrate (SAT) [Zhang et al., 1993; Middlebrook et al., 1993], there is also evidence showing that sulfuric acid droplets may remain liquid to the ice point [Koop et al., 1995; Iraci et al., 1995]. The most important pathways for the formation of PSC particles are thought to be: 1) direct deposition of nitric acid and water vapor on preexistent SAT to form NAT or NAD [Poole and McCormick, 1988; Zhang et al., 1996], 2) growth of liquid sulfate aerosol by the uptake of nitric acid and water to form LTA [Arnold, 1992; Carslaw et al., 1994; Tabazadeh et al., 1994], 3) freezing of ternary solution

<sup>1</sup>University of Wyoming, Laramie.

<sup>2</sup>Now at National Center for Atmospheric Research, Boulder, Colorado.

<sup>3</sup>Istituto di Fisica dell'Atmosfera, CNR, Rome.

<sup>4</sup>Norwegian Institute for Air Research, Tromsø, Norway.

<sup>5</sup>Service d'Aéronomie du CNRS, Verrières-le-Buisson, France.

Copyright 2000 by the American Geophysical Union.

Paper number 1999JD900469.  
0148-0227/00/1999JD900469\$09.00

droplets into NAT [Molina *et al.*, 1993; Iraci *et al.*, 1995], and 4) heterogeneous nucleation of nitric acid hydrates on ice [Koop *et al.*, 1995]. Other laboratory experiments show that formation of NAT on SAT is unlikely [Iraci *et al.*, 1995; Zhang *et al.*, 1996]; however, NAT may form from LTA on SAT if the SAT dissolves from the condensation of  $\text{HNO}_3$  and  $\text{H}_2\text{O}$  [Iraci *et al.*, 1998]. Experiments also show that ternary solution droplets readily supercool to temperatures approaching the ice point [Molina *et al.*, 1993; Anthony *et al.*, 1995; Koop *et al.*, 1997a]. This suggests that non ice PSCs may be composed primarily of ternary solution droplets and that NAT forms only when particles cool to the ice point [MacKenzie *et al.*, 1998], as may occur in lee waves [Meilinger *et al.*, 1995]. Other investigators, however, point to Arctic observations indicating that the duration of supercooling below the NAT point,  $T_{\text{NAT}}$ , may play a role in the development of NAT [Tabazadeh *et al.*, 1996; Larsen *et al.*, 1996] and that select nucleation and slow growth of NAT at temperatures below  $T_{\text{NAT}}$  should still be considered [Rosen *et al.*, 1997].

Laboratory measurements of  $\text{HNO}_3$  and  $\text{H}_2\text{O}$  condensation on thin films indicate that NAT is the most likely hydrate [Hanson and Mauersberger, 1988; Middlebrook *et al.*, 1993; Iraci *et al.*, 1994], while Worsnop *et al.* [1993] indicates that metastable dihydrates may form as a precursor to NAT. Other laboratory work, using vapor ratios of  $\text{HNO}_3/\text{H}_2\text{O}$  more representative of stratospheric conditions, suggests that PSCs may have  $\text{HNO}_3/\text{H}_2\text{O}$  compositions closer to a penta- or higher hydrate of  $\text{HNO}_3$  [Marti and Mauersberger, 1993].

Here we present simultaneous in situ and remote observations of two PSCs. We use these observations to investigate the index of refraction and volume of the PSC particles and compare these results with laboratory and theoretical estimates. The in situ measurements were made using an optical particle counter (OPC), a condensation nuclei (CN) counter, and a laser backscattersonde (LABS), and the remote measurements were

made using two lidars. The PSCs were observed in mid-January, 1996 and 1997, to the east of Andoya, Norway (69°N), between 20 and 25 km. The OPC and CN counter provide measurements of particle concentration in selected size bins between 0.01 and 5.0  $\mu\text{m}$ . LABS measures aerosol backscattering in situ at 692 and 830 nm. The lidar measurements are available at 308, 353, 532, and 1064 nm from Andoya. In 1996 measurements were available from the CN/OPC, from LABS, and at four lidar wavelengths. In 1997, measurements were obtained only from the CN/OPC and two lidar wavelengths.

## 2. Instrumentation

The aerosol counters measure the concentration of CN ( $r > 0.01 \mu\text{m}$ ) and optically detectable aerosol ( $r \geq 0.15\text{--}5.0 \mu\text{m}$ ). Following an original design by Rosen [1964], the OPCs count and size particles drawn into a scattering region. The size is determined from measurements of the intensity of scattered white light at 40° from the forward direction using Mie theory and assuming spherical particles with an index of refraction corresponding to sulfate, 1.45 [Hofmann and Deshler, 1991]. For CN the particles are forced to grow to optically detectable sizes with a growth chamber using ethylene glycol vapor. For aerosol  $\geq 0.15 \mu\text{m}$  radius the Poisson counting statistics for concentrations of 0.001–1.0  $\text{cm}^{-3}$  are 75–2%. For CN the uncertainties for concentrations of 1.0–10.0  $\text{cm}^{-3}$  are 8–3%.

Aerosol volume and surface area densities, or other distribution moments, are calculated by fitting either unimodal or bimodal lognormal size distributions to the cumulative concentration measurements [Hofmann and Deshler, 1991; Deshler *et al.*, 1993]. Example size distributions at three altitudes representative of different regions of the PSC observed in 1996 are shown in Figure 1. Uncertainties in measured concentrations due to counting statistics (see Figure 1) cause

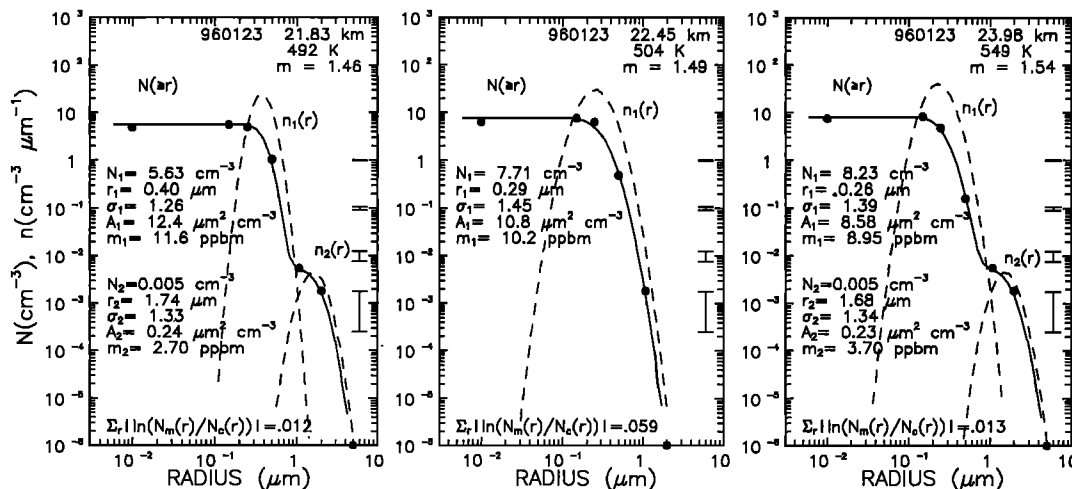


**Figure 1.** Unimodal/bimodal lognormal size distributions fit to optical particle counter measurements (solid circles) at three altitudes within the January 23, 1996, polar stratospheric cloud. The differential lognormal distributions for each mode are shown as dashed lines, and the cumulative concentration, from summing the integrals of the differential distributions, is shown as the solid lines. The parameters of the size distributions and the inferred surface areas and mass mixing ratios for  $\text{HNO}_3$ , assuming the particles are composed of nitric acid trihydrate, are shown. Uncertainties in the concentration measurements are shown by the vertical bars on the right-hand side. The goodness of the fit is shown at the bottom as the sum of the log of the ratios of measured and calculated number concentration. The measurements shown correspond to regions in the non-depolarizing region of the cloud with (21.83 km) and without (22.45 km) large particles, and in the depolarizing region (23.98 km).

average uncertainties in the distribution moments of 10-20%, with maxima of 50-60%, according to Monte Carlo simulations [Deshler *et al.*, 1993]. Uncertainties associated with using an index of refraction of 1.45 to estimate particle size can lead to a systematic sizing error of about 10%, dependent on the true refractive indices of the particles sampled. The index of refraction of sulfuric acid aerosol under typical stratospheric conditions is anticipated to be between 1.41 and 1.45 [Steele and Hamill, 1981], and for PSCs it is anticipated to be from 1.37 to 1.51 [Toon *et al.*, 1990; Berland *et al.*, 1994; Middlebrook *et al.*, 1994]. Variations of particle index of refraction in this range can cause underestimates of surface area and volume densities by an average of 5-10% with a standard deviation of 10-20% when compared with the estimates at 1.45. Combining the uncertainty of  $\pm 20\%$  due to counting statistics with an uncertainty of  $\pm 10\%$  due to uncertainties in index of refraction leads to average uncertainties of  $\pm 30\%$  on the derived moments of the aerosol size distributions measured by these counters [Deshler and Oltmans, 1998]. For the observations presented here, only the uncertainty related to counting statistics strictly applies, since a method is employed to estimate the particle indices of refraction. Counting statistics, however, provide the greater source of uncertainty.

The laser backscatter sonde LABS measures aerosol and molecular scattering and depolarization within 50 m of the balloon-borne gondola using lasers at wavelengths of 692 and 830 nm [Adriani *et al.*, 1999]. The emitted laser powers are 20 and 15 mW, respectively. The lasers are polarized by a factor of 100:1 and have a bandwidth of 1.0 nm. An on/off modulation of the laser emission provides sky background measurements which are subtracted from the backscattered signal. The laser beams are aligned nearly parallel with the telescope optical axis, and the telescope field of view has been set to collect light scattered at  $180^\circ \pm 1^\circ$  from the forward direction. The collected light is spectrally selected with a dichroic cube and filtered with interferential filters to a bandwidth of 10 nm. Since part of the light backscattered by aspherical particles is depolarized, the light at 692 nm is further split into its parallel and cross component, with respect to the initial state of polarization. The scattered light returned from the atmosphere, at photon counting rates, is measured with avalanche photodiodes. The photon counts are averaged over 10 s. An average balloon rise rate of  $5 \text{ m s}^{-1}$  gives a vertical resolution of 50 m for LABS profiles, which is equivalent to the OPC and CN measurements.

From LABS the ratio of total volume backscatter to molecular backscatter, backscattering ratio (BR), at two wavelengths is obtained versus altitude as the balloon rises. The backscattering coefficient is a function of the particle size distribution, particle refractive index, and the molecular density. The molecular signal is calculated from measurements of temperature and pressure. To estimate the signal from a pure molecular atmosphere, calibration factors are assessed at aerosol-free altitudes. In the present measurement, calibration altitudes have been taken at 7, at 15 and above 26 km, at the top of the sounding.

The uncertainty attributed to BR is mainly determined by photon counting statistics in the signal; however, uncertainties in measured pressure and temperature also contribute. Assuming an uncertainty in the signal due to fluctuations in photon counting statistics and uncertainties of 0.2 K for temperature and 0.5 hPa for pressure, an error of  $< 7\%$  is estimated for BR values to the top of the sounding.

The ratio between the depolarized and polarized signals at 692 nm (depolarization ratio) gives qualitative information about the

asphericity of the scattering particles and hence their thermodynamic phase. A molecular atmosphere is expected to give low depolarization, around 1.4%. This value has been confirmed both experimentally [Cohen and Low, 1969] and theoretically [Young, 1980]. In our measurement the depolarization ratio was normalized to its molecular value assuming that the ratio between the two channels was 1.4% in aerosol-free regions. Uncertainties of  $\pm 0.2$ -2.0% are given to the depolarization ratio in the range measured, 2-15%.

The ozone lidar at the Arctic Lidar Observatory for Middle Atmosphere Research (ALOMAR) at Andoya [Hoppe *et al.*, 1995] is a standard Differential Absorption Lidar (DIAL) system used widely for ozone measurements. It emits at two wavelengths: 308 nm, which is attenuated by about a factor of 10 because of extinction by atmospheric ozone, and 353 nm, which is virtually unaffected by ozone. The emission is produced by means of a pulsed XeCl excimer laser coupled with a hydrogen-filled Raman cell where about 15% of the laser emission is converted to 353 nm. The pulse length of the laser allows an optimal vertical resolution of 30 m; however, as a standard, 100-m vertical resolution is used in the measurements. The receiver system consists of a 1-m Newtonian telescope, a mechanical chopper cutting off the intense light from the troposphere, a variable shutter setting the receiver field of view to about 0.5 mrad, optical elements yielding moderate spectral filtering (about 2 nm), and photomultipliers in single-photon counting mode. The spectral filtering allows measurements at solar depression angles  $> 2^\circ$ . The system is run at a laser pulse repetition rate of 200 Hz with pulse energies between 100 and 150 mJ. In good weather this gives reliable ozone density profiles between 10 and 45 km with an integration time of about 1 hour. The same time is required for a temperature profile up to about 55 km. PSC profiles can be derived from each raw data file, with a time resolution of 5 minutes. Derivation of PSC properties without atmospheric Raman channels (which contain no aerosol scattering) in the instrument receiver requires a realistic aerosol-free reference profile. This can be obtained using temperature profiles from nearby radiosondes or from meteorological data from the European Centre for Medium-Range Weather Forecasts (ECMWF) or the U.K. Meteorological Office. For the 308-nm signal a representative ozone profile is needed as well. With such data given, Hansen *et al.* [1997] show that the backscatter ratios at both 353 and 308 nm can be derived with a high accuracy ( $\sigma_{BR} = 0.1$ -0.2), while the Ångström coefficient is much more sensitive to the reference profile used.

The ALOMAR Rayleigh/Mie lidar operates on the single, double, and triple wavelengths of a pulsed Nd-YAG laser with a 30-Hz repetition rate [Fierli *et al.*, 1998]. The emitted pulsed energy is 360, 400, and 215 mJ at wavelengths of 1064, 532, and 355 nm. The returned light is sampled with a 60-cm telescope. Backscattered light at the three wavelengths is detected with photon counting multipliers. The BR is normalized to 1.0 above the stratospheric aerosol layer. The uncertainty in BR is 10-15% for a 15-min integration.

### 3. Comparison Method

To infer PSC refractive indices from simultaneous size distribution and scattering measurements, the aerosol size distributions were used to calculate backscatter. The calculated backscatter was then compared with the measured backscatter at the six wavelengths used. For each wavelength the real part of the

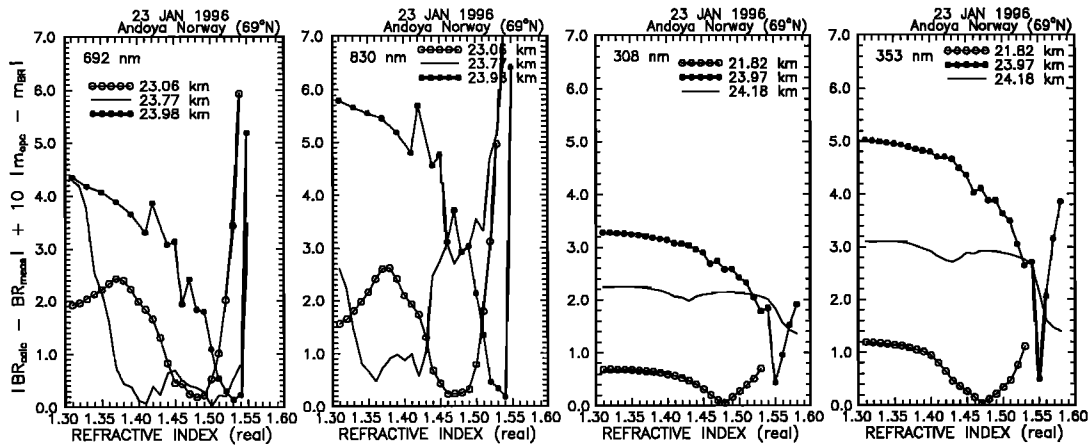


**Figure 2.** As a function of  $m_{\text{OPC}}$ , the difference of calculated and measured backscattering ratio plus 10 times the difference between the index assumed for the OPC sizes ( $m_{\text{OPC}}$ ) and that assumed for the backscattering calculations ( $m_{\text{BR}}$ ). These are for comparisons on January 23, 1996, at three altitudes for 692 and 830 nm and three altitudes for 308 and 353 nm. Altitude levels shown with connected data symbols were accepted as valid determinations of index of refraction, while those with only a line were rejected.

particle index of refraction ( $m_{\text{OPC}}$ ) was varied between 1.31 and 1.60 using steps of 0.01. Absorption is negligible at wavelengths between 308 and 1064 nm; thus the imaginary part of refractive index is negligible. At a forward scattering angle of  $40^\circ$  the response of the OPC is monotonic with particle size for the refractive indices considered [Hofmann and Deshler, 1991]. For each  $m_{\text{OPC}}$  the OPC sizes were adjusted to reflect the change in counter response as a function of index of refraction, and the measured concentrations at the new sizes were fit with unimodal/bimodal lognormal size distributions. Aerosol backscattering was then calculated at each wavelength for a set of refractive indices,  $m_{\text{BR}} = m_{\text{OPC}} \pm 0.04$ , surrounding the index assumed for the OPC measurements. A step size of 0.01 was also used, but  $m_{\text{BR}}$  was limited to the range  $1.30 \leq m_{\text{BR}} \leq 1.60$ . The index,  $m_{\text{BR}}$ , providing the best match between the calculated and measured backscattering is assumed to be representative of the PSCs measured, but only if the minimum in the difference between calculated and measured BR is well defined. This is the same technique as used in the analysis of Antarctic data by Adriani *et al.* [1995].

To quantify this method,  $m_{\text{OPC}}$  and  $m_{\text{BR}}$  were varied to minimize the error function defined as  $|BR_{\text{calc}} - BR_{\text{meas}}| + w |m_{\text{OPC}} - m_{\text{BR}}|$ .  $BR_{\text{calc}}$  and  $BR_{\text{meas}}$  are the calculated and measured BR,  $w$  is a weighting factor, taken as 10, to preclude large differences between  $m_{\text{OPC}}$  and  $m_{\text{BR}}$ . For these calculations,  $m_{\text{OPC}}$  is varied through the range 1.30–1.60 with  $m_{\text{BR}} = m_{\text{OPC}} \pm 0.04$  but constrained to be between 1.30 and 1.60. The value of  $w$  was chosen somewhat arbitrarily, and sensitivity tests were not completed to test the importance of this value. We felt that  $w$  should be large enough to provide a reasonably strong constraint on the deviation of  $m_{\text{BR}}$  from  $m_{\text{OPC}}$ . The value of 10 satisfied this requirement. Only indices of refraction which were well defined by this error function were included in the results. Examples of the variation of the error function as a function of  $m_{\text{OPC}}$  are shown in Figure 2 for three comparisons at 692 and 830 nm and three comparisons at 308 and 353 nm. The error function is plotted as a function of  $m_{\text{OPC}}$  to present these graphs as single-valued functions of  $m$ . The error function can have a multivalued dependence on  $m_{\text{BR}}$ . Thus, since  $m_{\text{BR}}$  is used to specify the value

of index of refraction for the PSCs measured, the minimum index of refraction shown in Figure 2 may not coincide with the index of refraction inferred for the PSC measurements, but the deviation will be less than 0.04 and is usually less than 0.02. For 692 and 830 nm the comparison at 23.77 km was rejected, and the comparisons at 23.06 and 23.98 km were accepted. At 692 nm, two minimums are defined at 23.77 km, and at 830 nm the minimum is too broad. For the ozone lidar comparisons at 308 and 353 nm no minimum was found at 24.18 km, while the comparisons at 21.82 and 23.97 km give good results. In most cases, altitudes rejected at one wavelength were also rejected at other wavelengths. Roughly 40% of the comparisons were rejected because of a poorly defined minimum in  $m_{\text{OPC}}$ . In the majority of rejected comparisons the error function displayed little sensitivity to index of refraction, as in the cases rejected at 308 and 353 nm in Figure 2. Only in a few cases were two minimums defined.

An error analysis of the method to infer index of refraction was completed using a Monte Carlo simulation to allow aerosol number concentration  $N$ , radius, and BR to all vary within their uncertainty limits of  $\pm 1/\sqrt{N}$ ,  $\pm 10\%$ , and  $\pm 10\%$ , respectively. For these calculations the same constraints as above were placed on  $m_{\text{BR}}$  and  $m_{\text{OPC}}$ . With these uncertainty limits applied to a set of observations at one altitude, the Monte Carlo population of inferred indices of refraction had a standard deviation of  $\pm 0.03$  for indices in the range 1.30–1.60.

## 4. Observations

### 4.1. January 23, 1996

In the period January 22–24, 1996, a strong polar vortex was centered near the North Pole and elongated along the  $90^\circ\text{E}/90^\circ\text{W}$  meridians. The ECMWF analysis indicates that below the 475-K potential temperature ( $\theta$ ) surface ( $\sim 21$  km), the vortex edge was several hundred kilometers north of Andoya. Above this the vortex edge passed over Andoya, and at  $\theta = 550$  K ( $\sim 24$  km) and 675 K ( $\sim 28$  km) the vortex edge was south of Andoya. Back trajectories based on the ECMWF analysis indicate that air

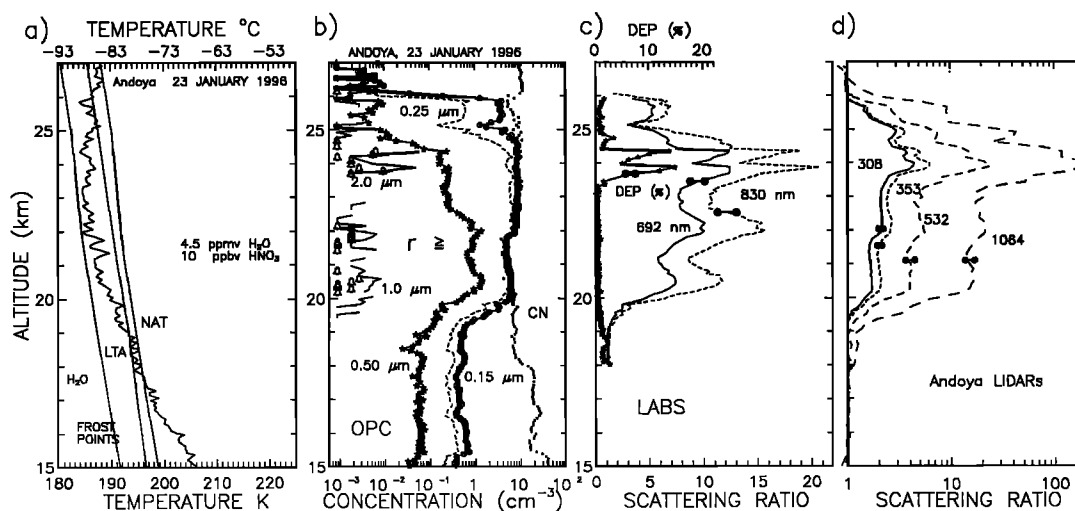


**Figure 3.** Measurements on January 23, 1996, near Andoya, Norway (69°N), of (a) temperature, (b) aerosol concentration for particles with radius  $\geq 0.01$  (CN), 0.15, 0.25, 0.50, 1.0, and 2.0  $\mu\text{m}$ , (c) in situ backscattering and depolarization ratio at 692 and BR at 830 nm, and (d) lidar BR at 308, 353, 532, and 1064 nm. The temperature measurements are compared to equilibrium temperatures for NAT [Hanson and Mauersberger, 1988] for liquid ternary aerosol [Carslaw et al., 1994], and for water ice, assuming 4.5 ppmv  $\text{H}_2\text{O}$  and 10 ppbv  $\text{HNO}_3$ . The symbols used for the large particles from the OPC measurements are 1.0  $\mu\text{m}$  (solid line) and 2.0  $\mu\text{m}$  (bells, no line). Sample error bars are shown on the aerosol scattering and depolarization measurements.

parcels above  $\theta = 500$  K ( $\sim 22$  km) resided within the polar vortex for at least 10 days prior to January 23. Above  $\theta = 475$  K a large cold cell was centered over northern Norway. At lower altitudes the center of cold air was north of Finland. Minimum temperatures over Andoya were measured at 184–186 K between 22 and 26 km, below  $T_{\text{NAT}}$  for 4 ppmv  $\text{H}_2\text{O}$  and 5 ppbv  $\text{HNO}_3$ . A warm cell with temperatures approaching 233 K was positioned on the opposite side of the Northern Hemisphere, north of Japan.

On January 23, 1996, a thick PSC was observed above Andoya. A balloon, carrying the CN, OPC, and LABS instruments, was released from Andoya Rocket Range (69°N, 16°E) at 1800 UT and passed through the PSC at altitudes between 20 and 25 km at  $\sim 1900$  UT. Aerosol BR from this same PSC at 308, 353, 532, and 1064 nm was observed at Andoya with two lidars. The lidar measurements bracketed the time of the in situ measurements. Figure 3 displays the temperature, aerosol concentration, and BRs observed between 15 and 27 km. The temperatures are compared with existence temperatures calculated for NAT [Hanson and Mauersberger, 1988], LTA [Carslaw et al., 1995], and ice, assuming 4.5 ppmv  $\text{H}_2\text{O}$  and 10 ppbv  $\text{HNO}_3$ . The LTA temperatures were selected, somewhat arbitrarily, as the temperature where significant volume change begins to occur during the growth of LTA. Stratospheric water vapor mixing ratios of 4 ppmv were observed above Sodankylä, Finland, early in the morning of January 23 with a frost point hygrometer [Vömel et al., 1997].

Increases in particle concentration for particles  $\geq 0.15$   $\mu\text{m}$  begin near 19 km as the temperature approaches  $T_{\text{LTA}}$  (Figures 3a and 3b). Temperature cools to the ice point (for 4.5 ppmv  $\text{H}_2\text{O}$ ) between 20 and 25 km, which corresponds to the thickest portion of the PSC. Aerosol concentrations return to those expected for stratospheric sulfuric acid aerosol above 26 km as the temperature warms above  $T_{\text{NAT}}$ . Water vapor measurements on January 23 at 0000 UT from Sodankylä indicated a region between 21.5 and 24.3 km where a significant water vapor deficit

was evident [Vömel et al., 1997]. Water vapor was reduced to 2.5 ppmv, suggesting that ice clouds were present between Andoya and Sodankylä or that ice clouds had occurred prior to our measurements near 1800 UT. The ozone lidar, which was operational from 1430 UT, showed a narrow layer at 23–24 km with enhanced backscatter ratio and Ångström coefficient beginning at 1500 UT. The layer was at first patchy and then developed into a triple layer at about 1700 UT, with maximum backscatter ratios occurring near 1800 UT. Hansen and Hoppe [1997] provide additional details concerning the temporal development of this cloud. The largest particles observed on January 23 with the OPC were narrow layers of 2.0- $\mu\text{m}$  particles at 20–21 km and at 23.5–24 km, while particles as large as 1.0  $\mu\text{m}$  were observed throughout the cloud; however, the aerosol volumes and backscatter were too low to suggest ice. Although these particle sizes are consistent with the largest observed sizes suggested by backscattersonde measurements from Sodankylä [Vömel et al., 1997], the condensed ice volumes observed near Andoya were significantly less than observed near Sodankylä.

Between 19 and 20 km the concentrations of aerosol at the lowest sizes, 0.15 and 0.25  $\mu\text{m}$ , increase to match the CN concentration, indicating that the entire aerosol population experienced condensational growth. This coincidence of the concentration of larger aerosol with CN within a PSC is somewhat common in the Arctic [Hofmann et al., 1990, Deshler and Oltmans, 1998] but is rarely observed in the Antarctic [Deshler et al., 1991].

The aerosol BRs are shown in Figures 3c and 3d. The in situ measurements from LABS are shown in Figure 3c, including a depolarization signal, and the four wavelengths measured at Andoya are shown in Figure 3d. To select the best lidar data for these comparisons, average wind speeds between 15 and 25 km were used to determine the approximate time the air parcels sampled by the balloon-borne instruments passed over the lidar site, or over a line orthogonal to the mean winds and passing

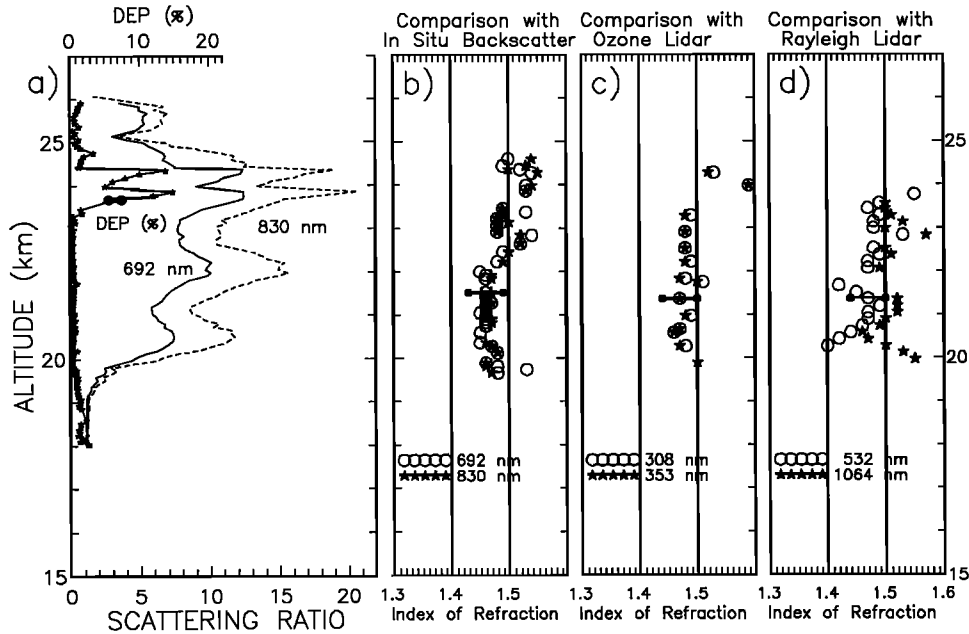


**Figure 4.** Indices of refraction inferred from a comparison of the measured BRs with those calculated from the OPC data. The comparisons are with (b) laser backscatter on LABS, (c) ozone lidar, and (d) Rayleigh lidar. The altitude resolutions are  $\sim 50$  m for the OPC/LABS comparison and  $\sim 100$  m for the OPC/lidar comparisons. For reference, Figure 4a gives BR at 692 and 830 nm and the depolarization ratio at 692 nm measured in situ with LABS. Example error bars near 21 km indicate the precision of the index of refraction determination based on the measurement uncertainty of the instruments.

through Andoya. With this method the lidar measurements most closely coinciding with the in situ measurements between 15 and 25 km were made between 1755 and 1826 UT. The vertical structure of the PSC is reproduced in all six BR measurements, both in situ and remote, indicating the PSC was horizontally homogeneous. The two primary peaks at 24 km are seen in all scattering ratio data and in the  $1.0\text{-}\mu\text{m}$  concentrations from the OPC. This is also the only region of the cloud exhibiting depolarization, indicating the presence of nonspherical particles.

To infer particle index of refraction, the size distribution measurements were used to calculate aerosol scattering as a function of  $m$ , using the method outlined above. The true  $m$  is assumed to coincide with that value of  $m_{\text{BR}}$  which minimizes the error function defined previously. Because of the weighting to keep  $m_{\text{BR}}$  and  $m_{\text{OPC}}$  close, the final  $\text{BR}_{\text{calc}}$  may at times deviate somewhat from the closest match to  $\text{BR}_{\text{meas}}$ .

The values of  $m_{\text{BR}}$  inferred from the comparison of aerosol size distribution data and the BRs measured at six wavelengths are shown in Figure 4. The results are quite encouraging, especially for the comparisons with LABS and with the ozone lidar. In both of these cases the comparison at two wavelengths produced nearly the same index of refraction suggesting that the method is internally self-consistent. Between 20 and 23 km the average and standard deviation of the indices inferred using LABS was  $1.47 \pm 0.02$  and using the ozone lidar was  $1.48 \pm 0.01$ . In the depolarizing portion of the PSC, 23.5–24.5 km, the index increased to  $>1.5$  for both the LABS and ozone lidar data. The comparison with the Rayleigh lidar produced roughly a similar picture, but the data were not as self-consistent at 532 and 1064 nm, and there was much more scatter in the refractive indices inferred. In a separate analysis of these data, *Mehrtens et al.* [1999] used backscattering at three wavelengths, 355, 532,

and 1064 nm, to infer monomodal aerosol size distributions and thus aerosol volume. *Mehrtens et al.* compared the inferred aerosol volume over a range of indices of refraction with aerosol volumes from the OPC measurements. The best comparisons were found for an index of refraction of 1.45. This result is at the lower range of the indices of refraction inferred here.

Back trajectories calculated from the ECMWF analyses indicate that the air between  $\theta = 425$  K ( $\sim 18$  km) and 675 K was cooling continuously for the previous 2 days from between 210 and 220 K to  $T_{\text{NAT}}$ , a cooling rate of  $\sim 10$  K  $\text{d}^{-1}$ . In back trajectories at different levels a significant difference was observed in the maximum temperatures experienced in the previous 10 days. Below  $\theta = 525$  K the air parcels experienced maximum temperatures above 215 K four days prior to observation, while at  $\theta = 525$  K and above, the temperatures remained below 215 K for the previous 10 days. Also, air parcels between  $\theta = 500$  and 575 K all experienced temperatures below 190 K approximately 6 days prior to observation. Air parcels above and below these levels did not experience such low temperatures. Thus, between  $\theta = 525$  K ( $\sim 23$  km) and 575 K ( $\sim 25$  km) there is a chance that at least some of the sulfate aerosol on which the PSC formed was SAT. This was not a possibility below  $\theta = 525$  K, where temperatures above the melting point of SAT [*Middlebrook et al.*, 1993] had been experienced since the last encounter with PSC temperatures. Thus these trajectories are consistent with the idea that nitric acid hydrates are more likely to form on SAT, while LTA are expected on liquid sulfuric acid aerosol [*Tabazadeh et al.*, 1995].

#### 4.2. January 19, 1997

In the period January 18–20, 1997, the polar vortex encompassed northern Norway, including Andoya. The vortex

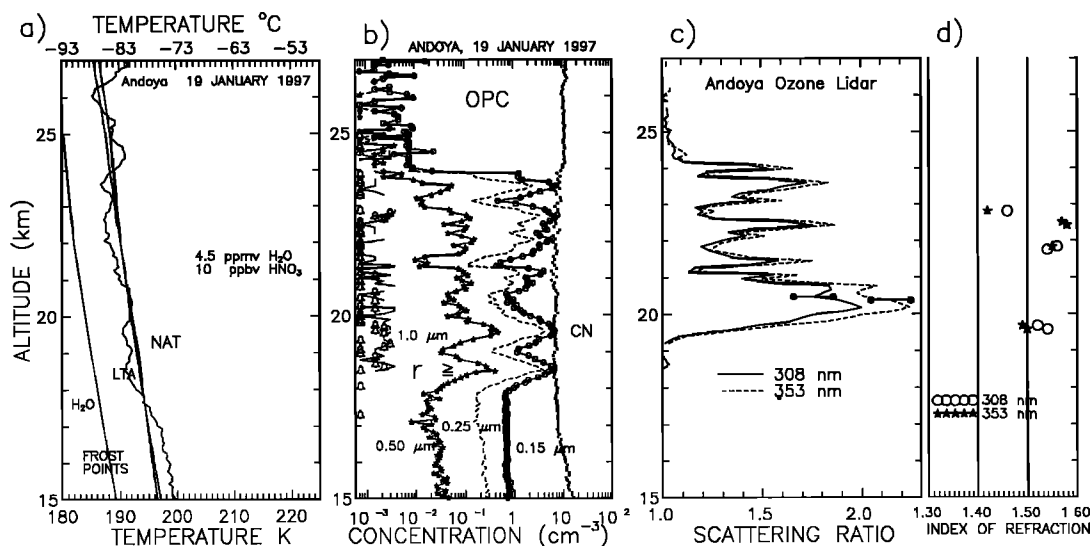


**Figure 5.** Measurements on January 19, 1997, near Andoya, Norway ( $69^{\circ}\text{N}$ ), of (a) temperature, (b) aerosol concentration for particles with radius  $\geq 0.01$  (CN), 0.15, 0.25, 0.50, 1.0 and 2.0  $\mu\text{m}$ , (c) lidar BR at 308 and 353 nm, and (d) inferred index of refraction from the comparison of the OPC and lidar data. The temperature measurements are compared to equilibrium temperatures for NAT [Hanson and Mauersberger, 1988], for LTA [Carlsaw *et al.*, 1994], and for water ice, assuming 4.5 ppmv  $\text{H}_2\text{O}$  and 10 ppbv  $\text{HNO}_3$ . The symbols used for the large particles from the OPC measurements are 1.0  $\mu\text{m}$  (solid line) and 2.0  $\mu\text{m}$  (bells, no line). Sample error bars are shown on the aerosol scattering measurements.

was centered approximately 1000 km northeast of Andoya at about  $75^{\circ}\text{N}$ . The segment of the vortex edge nearest Andoya was about 1000 km to the southwest. The vortex was slightly distorted into a teardrop shape, with the sharp apex over northeastern Canada. The pool of cold air moved westward over Norway with the center of the cold air at all levels above  $\theta = 435$  K over northern Norway on January 19, 1997. A minimum temperature of 186 K was measured over Andoya at 26 km. A warm cell with temperatures reaching 228 K was positioned on the opposite side of the northern hemisphere over eastern Siberia. Back trajectories indicate that above  $\theta = 450$  K ( $\sim 19$  km), air parcels over Andoya remained within the vortex for at least 10 days prior to the measurement.

On January 19, 1997, another strong PSC, at roughly the same altitude as in 1996, was measured with the OPC and at two lidar wavelengths. In contrast to 1996, this PSC displayed significant vertical structure. Temperatures were not as cold as in 1996. In 1997, LABS was not available, so only a comparison between the in situ OPC and remote lidar measurements was possible. Figure 5 shows the observations and the results of the comparison between OPC and ozone lidar. Again, in this PSC, there are layers where the complete CN population has been activated to grow within the PSC. These are evident in the layers where the concentration of 0.15 and 0.25  $\mu\text{m}$  particles match the CN concentrations. The peaks in concentration at 0.15- and 0.25- $\mu\text{m}$  also follow the vertical structure in the temperature profile, showing an anticorrelation with temperature.

The comparison of in situ aerosol size distribution measurements and remote ozone lidar observations is disappointing. Unique refractive indices were identified in only a few comparisons. We believe that the strong vertical structure prevented a useful comparison based on altitude between the remote and in situ data since the peaks in scattering and particle concentration often do not coincide.

## 5. Discussion

A summary of the indices of refraction inferred from the comparison of size distribution and scattering measurements on January 23, 1996, at the six different wavelengths is shown in Figure 6. The PSC was divided into a nondepolarizing (20–23.3 km) region and a depolarizing (23.4–24.5 km) region, and the indices of refraction inferred in each region and at each wavelength were averaged. The error bars shown in Figure 6 represent the population standard deviation at each wavelength and in each cloud region. Also shown are a similar comparison between OPC and lidar (532 nm) measurements in Antarctica [Adriani *et al.*, 1995], laboratory measurements at 650 nm for nitric acid monohydrate and NAD [Berland *et al.*, 1994] and NAT [Middlebrook *et al.*, 1994], laboratory measurements at 308 and 365 nm for LTA [Beyer *et al.*, 1996], and theoretical estimates for LTA [Luo *et al.*, 1996]. The Lorentz-Lorenz relationship [Born and Wolf, 1975] is used along with Beyer *et al.*'s [1996] constants for ternary solutions to obtain the refractive indices at 308 and 365 nm for LTA at temperatures near 190 K.

All wavelengths below 850 nm are consistent in showing an increase in index of refraction in the upper depolarizing cloud. In the nondepolarizing cloud the comparisons with LABS and the ozone lidar show the least dispersion. The values of index of refraction in the nondepolarizing cloud are consistent with the laboratory measurements for NAT, whereas the measurements in the depolarizing cloud are more consistent with laboratory measurements on NAD.

At wavelengths between 530 and 850 nm the index of refraction increases by  $\sim 0.04$  in the depolarizing portion of the cloud where nonspherical particles are present. At the UV wavelengths the increase in inferred index of refraction is about 0.08. Nonspherical particles may cause sizing errors in the OPC,

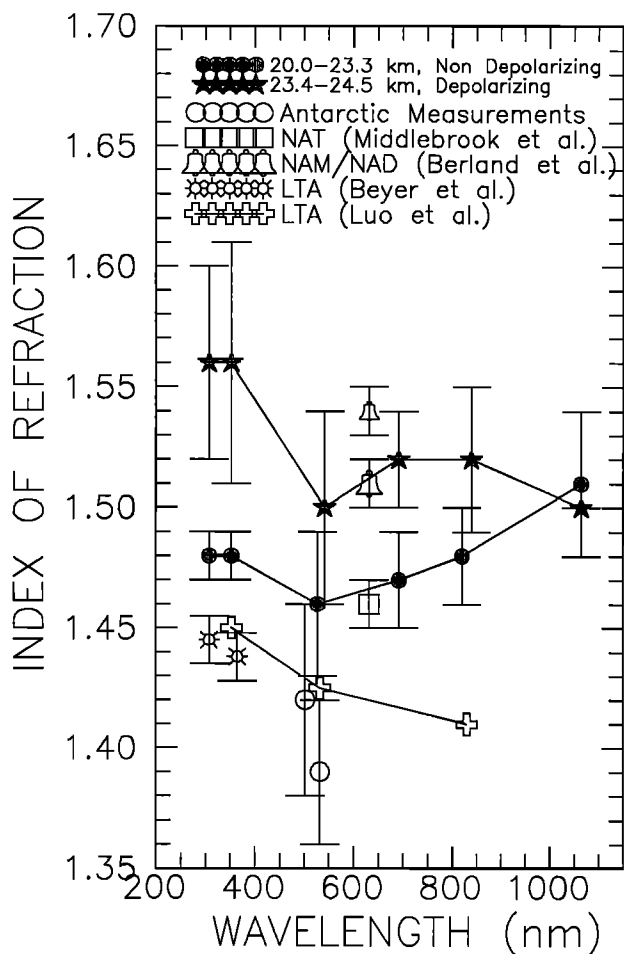


**Figure 6.** Index of refraction as a function of wavelength. The indices calculated here from a comparison of aerosol concentration and BR data are shown for the six wavelengths measured as a mean and population standard deviation for observations in the nondepolarizing (20–23.3 km) and depolarizing (23.4–24.5 km) cloud. Also shown are comparisons between OPC and lidar data in Antarctica [Adriani *et al.*, 1995] (open circles); laboratory measurements on thin films of nitric acid monohydrate (NAM) and nitric acid dihydrate (NAD) [Berland *et al.*, 1994] (bells), NAT [Middlebrook *et al.*, 1994] (box), LTA [Beyer *et al.*, 1996] (suns), and theoretical calculations for LTA [Luo *et al.*, 1996] (open crosses). The wavelengths for some measurements are shifted slightly to improve readability of the error bars.

which uses Mie theory to determine particle size. Mishchenko *et al.* [1996] reviewed the effect of nonspherical particles on light scattering using  $T$  matrix calculations. The effective radius, the ratio of aerosol volume to surface area, for the size distributions inferred from the OPC in the depolarizing region of the cloud ranged from 0.15–0.18  $\mu\text{m}$ . This coincides with an effective size parameter of 1.0–3.0 for the range of wavelengths used in the white light counter, 0.3–0.7  $\mu\text{m}$ . At the forward scattering angle of  $40^\circ$  used in the OPC, Mishchenko *et al.*'s calculations indicate that for size parameters of 1–3, there is no change in the phase function of either oblate or prolate spheroids compared to surface equivalent spheres. Thus the size measurements used here which assume spherical particles and Mie theory should not have large uncertainties.

To further characterize the PSCs, Figure 7 compares the observed aerosol volumes with those expected on the basis of thermodynamic calculations [Hanson and Mauersberger, 1988; Carslaw *et al.*, 1995]. At the base of the PSC on January 23, 1996, the observed volumes closely match the predictions for LTA, even for the fine-scale features which result from structure in the temperature profile. Between 20.5 and 23 km the observations are consistent with both LTA and NAT. Above 23 km the theoretical volumes diverge as the temperature warms and LTA decreases. In this region the observations remain near the higher volumes expected for NAT. This corresponds with the depolarizing region of the cloud, which is consistent with the common idea that NAT particles appear in depolarizing PSCs.

PSC volumes inferred from the observations on January 19, 1997 (Figure 7), display some layered structure but not as strongly as observed in the concentration of the smaller particles measured. The observed aerosol volumes are not clearly consistent with either LTA or NAT; however, the observed volumes are closer to NAT between 20 and 24 km, while LTA indicates only narrow layers of growth at 18.5 and 22.5 km. The few indices of refraction reported for this day (Figure 5) were  $> 1.5$ , which is more consistent with the depolarizing portion of the cloud on January 23, 1996.

Back trajectories using the ECMWF analyses indicate that, like January 23, 1996, the air between  $\theta = 400$  and 675 K was cooling continuously in the previous 2 days. The minimum temperatures reached in the previous 10 days approached 190 K only between  $\theta = 500$  and 550 K, and maximum temperatures remained below  $T_{\text{SAT}}$  only for air parcels above  $\theta = 475$  K ( $\sim 21$  km). Comparing observed and calculated aerosol volumes (Figure 7) does not suggest a broad distinction between NAT and LTA based on differences in temperature history above and below  $\theta = 475$  K. Thus no simple connections can be made between particle temperature history and particle type on January 19, 1997.

## 6. Summary and Conclusions

A method was applied to infer particle index of refraction within polar stratospheric clouds on the basis of comparing backscattering and size-resolved aerosol concentration measurements. The precision of this method, accounting for errors in individual measurements, was estimated to be  $\pm 0.03$  over the index of refraction range 1.30–1.60. The method was applied to PSCs observed above Norway on January 23, 1996, and January 19, 1997.

In 1996 a vertically and horizontally homogeneous PSC with temperatures near the ice point was observed between 20 and 26 km using both in situ and remote measurements. A comparison of size-resolved number concentration measurements with 1) in situ backscattering at two wavelengths and 2) remote backscattering at four wavelengths suggests that the index of refraction of the PSC particles is near  $1.47 \pm 0.01$  in the nonpolarizing region of the cloud and  $1.52$ – $1.56 \pm 0.04$  in the depolarizing region. These values are higher than expected on the basis of laboratory measurements [Berland *et al.*, 1994; Middlebrook *et al.*, 1994; Beyer *et al.*, 1996], measurements in Antarctica [Adriani *et al.*, 1995], and theory [Luo *et al.*, 1996] but are consistent across four of the six wavelengths used in the measurements here: the comparison with in situ backscattering and with measurements using the ozone lidar. The comparisons with the Rayleigh lidar are not as consistent. The disagreement between the index of

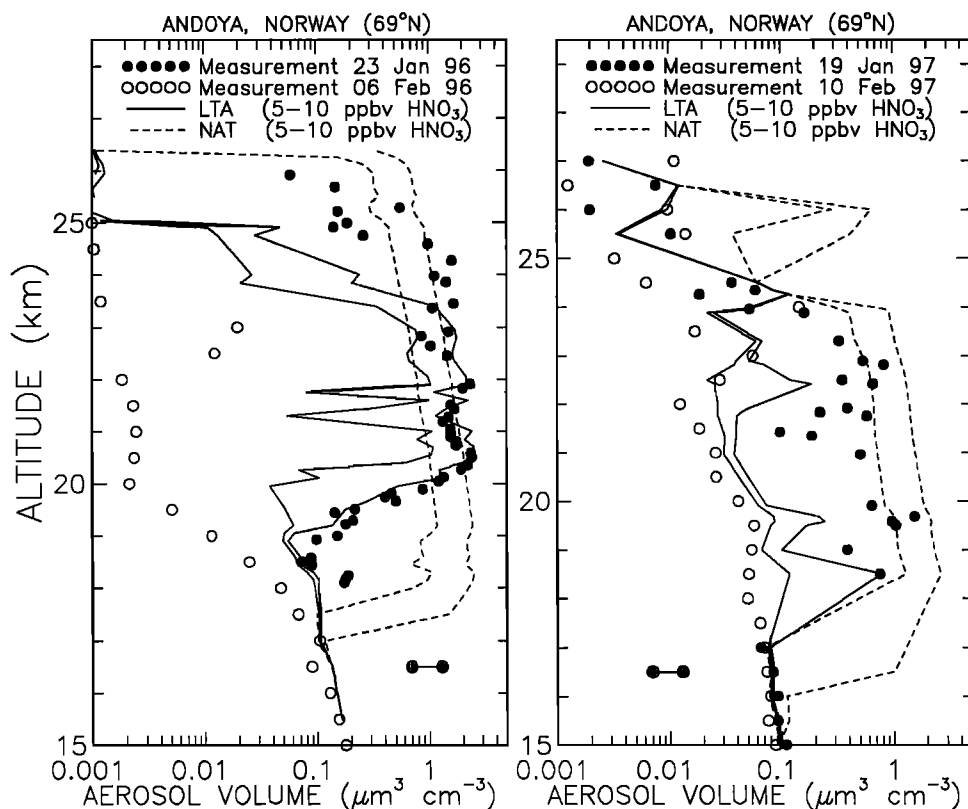


**Figure 7.** (a) Vertical profiles of aerosol volume for sulfate on February 6, 1996 (open circles), and PSCs on January 23, 1996 (solid circles). (b) Aerosol volume for sulfate on February 10, 1997 (open circles), and for PSCs on January 19, 1997 (solid circles). In Figures 7a and 7b a range of theoretical aerosol volumes for NAT and LTA [Carlsaw *et al.*, 1994] is calculated assuming 4.5 ppmv  $H_2O$  and 5-10 ppbv  $HNO_3$ . For the calculated volumes the sulfuric acid mixing ratio profile is inferred from the measured aerosol volumes for the non-PSC case in each year, February 6, 1996, and February 10, 1997. Representative error bars of  $\pm 30\%$  are shown at the bottom of each panel.

refraction inferred here for LTA and that expected on the basis of laboratory and theoretical work is troubling and at this point unexplained. The observed aerosol volumes agree closely with volumes expected for LTA, assuming 4.5 ppmv  $H_2O$  and 10 ppbv  $HNO_3$ , at the base of the cloud. Within the lower nondepolarizing portion of the cloud the observed LTA and NAT volumes all agree, while above 23 km, in the depolarizing region, the observed volumes agree only with NAT.

In 1997 a PSC between 18 and 25 km with strong vertical structure was observed in situ with optical particle counters and remotely with lidar at 308 and 353 nm. Comparing these measurements did not result in a clear index of refraction. This is at least partially explained by the strong vertical structure observed on this day, leading to a horizontally inhomogeneous PSC. Since the only aerosol scattering measurements available in 1997 were from lidar,  $\sim 50$  km from the in situ measurements, the horizontal and vertical structure inherently limits comparisons between these measurements based on altitude. Comparisons of observed and theoretical aerosol volumes, assuming 4.5 ppmv  $H_2O$  and 10 ppbv  $HNO_3$ , suggest that this PSC was composed primarily of NAT. At the temperatures observed, theoretical volumes for LTA evidenced little growth beyond sulfate volumes.

This method, using aerosol size distribution and scattering measurements from in situ instruments collocated on a balloon,

appears to be a useful tool to infer aerosol index of refraction and hence composition. This method can be applied with equal success to compare in situ and remote lidar measurements only in cases where the PSC has a broad horizontal extent with little vertical structure.

**Acknowledgments.** The authors would like to thank the many technical people involved in these measurements both at Andoya Rocket Range and at our home institutions. Without their devoted efforts this work could not have been completed. The research was supported by grants from the U. S. National Science Foundation, the European Union, and Italian, German, and French national agencies.

## References

- Adriani, A., T. Deshler, G. Di Donfrancesco, G. P. Gobbi, Polar stratospheric clouds and volcanic aerosol during spring 1992 over McMurdo Station, Antarctica: Lidar and particle counter comparisons, *J. Geophys. Res.*, **100**, 25877-25897, 1995.
- Adriani A., F. Cairo, L. Pulvirenti, F. Cardillo, M. Viterbini, G. Di Donfrancesco, and J.P. Pommereau, Stratospheric background aerosol and polar clouds observations by laser backscatter-sonde in the frame of the European project Stratospheric Regular Sounding, *Ann. Geophys.*, **17**, 1352-1360, 1999.
- Anthony, S. E., R. T. Tisdale, R. S. Disselkamp, M. A. Tolbert, and J. C. Wilson, FTIR studies of low temperature sulfuric acid aerosols, *Geophys. Res. Lett.*, **22**, 1105-1108, 1995.
- Arnold, F., Stratospheric aerosol increases and ozone destruction:

- Implications from mass spectrometer measurements, *Ber. Bunsen. Phys. Chem.*, **96**, 339-350, 1992.
- Berland, B. S., D.R. Haynes, K.L. Foster, M.A. Tolbert, S.M. George, and O.B. Toon, Refractive indices of amorphous and crystalline  $\text{HNO}_3/\text{H}_2\text{O}$  films representative of polar stratospheric clouds, *J. Phys. Chem.*, **98**, 4358-4364, 1994.
- Beyer, K. D., A. R. Ravishankara, and E. R. Lovejoy, Measurements of UV refractive indices and densities of  $\text{H}_2\text{SO}_4/\text{H}_2\text{O}$  and  $\text{H}_2\text{SO}_4/\text{HNO}_3/\text{H}_2\text{O}$  solutions, *J. Geophys. Res.*, **101**, 14519-14524, 1996.
- Born, M., and E. Wolf, *Principles of Optics*, Pergamon, Tarrytown, N. Y., 1975.
- Carslaw, K. S., B. P. Luo, S. L. Clegg, Th. Peter, P. Brimblecombe and P. J. Crutzen, Stratospheric aerosol growth and  $\text{HNO}_3$  gas phase depletion from coupled  $\text{HNO}_3$  and water uptake by liquid particles, *Geophys. Res. Lett.*, **21**, 2479-2482, 1994.
- Carslaw, K. S., B. Luo, and Th. Peter, An analytic expression for the composition of aqueous  $\text{HNO}_3$ - $\text{H}_2\text{SO}_4$  stratospheric aerosols including gas phase removal of  $\text{HNO}_3$ , *Geophys. Res. Lett.*, **22**, 1877-1880, 1995.
- Cohen, A. J., and W. Low, An experimental determination of the depolarization of scattered laser light by atmospheric air, *J. Appl. Meteorol.*, **8**, 952-954, 1969.
- Crutzen, P. J., and F. Arnold, Nitric acid cloud formation in the cold Antarctic stratosphere: A major cause for the springtime "ozone hole", *Nature*, **324**, 651-655, 1986.
- Del Negro, L. A., et al., Evaluating the role of NAT, NAD, and liquid  $\text{H}_2\text{SO}_4/\text{H}_2\text{O}/\text{HNO}_3$  solutions in Antarctic polar stratospheric cloud aerosol: Observations and implications, *J. Geophys. Res.*, **102**, 13,255-13,282, 1997.
- Deshler, T., and S. J. Oltmans, Vertical profiles of volcanic aerosol and polar stratospheric clouds above Kiruna, Sweden, winters 1993 and 1995, *J. Atmos. Chem.*, **30**, 11-23, 1998.
- Deshler, T., A. Adriani, D. J. Hofmann, and G. P. Gobbi, Evidence for denitrification in the 1990 Antarctic spring stratosphere: II Lidar and aerosol measurements, *Geophys. Res. Lett.*, **18**, 1999-2002, 1991.
- Deshler, T., B. J. Johnson, and W. R. Rozier, Balloonborne measurements of Pinatubo aerosol during 1991 and 1992 at 41 °N: Vertical profiles, size distribution, and volatility, *Geophys. Res. Lett.*, **20**, 1435-1438, 1993.
- Dye, J. E., D. Baumgardner, B. W. Gandrud, S. R. Kawa, K. K. Kelly, M. Loewenstein, G. V. Ferry, K. R. Chan, and B. L. Gary, Particle size distributions in Arctic polar stratospheric clouds, growth and freezing of sulfuric acid droplets, and implications for cloud formation, *J. Geophys. Res.*, **97**, 8015-8034, 1992.
- Dye, J. E., et al., In-situ observations of an Antarctic polar stratospheric cloud: Similarities with Arctic observations, *Geophys. Res. Lett.*, **23**, 1913-1916, 1996.
- Fahey, D. W., K. K. Kelly, G. V. Ferry, L. R. Poole, J. C. Wilson, D. M. Murphy, M. Loewenstein, K. R. Chan, In situ measurements of total reactive nitrogen, total water, and aerosol in a polar stratospheric cloud in the Antarctic, *J. Geophys. Res.*, **94**, 11,299-11,315, 1989.
- Fierli, F., A. Hauchecorne, D. Nedeljkovic, H. Mehrtens, U. Von Zahn, and K. H. Fricke, Relationship between PSC and Temperature measured by ALOMAR R/M/R lidar at Andoya, Proceedings of XVIII Quadriennial Ozone Symposium, L'Aquila, Italy, edited by R. Bojkov and G. Visconti, pp. 503-506, Pubbl. del Parco Tecnol. d'Abruzzo, Atto, Italy 1998.
- Hansen, G., and U. -P. Hoppe, Lidar observations of polar stratospheric clouds and stratospheric temperature in winter 1995/96 over northern Norway, *Geophys. Res. Lett.*, **24**, 131-134, 1997.
- Hansen, G., U.-P. Hoppe, B. Nardi and T. Deshler, Ozone lidar analysis technique: Combining balloon data with lidar measurements, paper presented at ESA Symposium on European Rocket and Balloon Progress and Related Research, Eur. Space Agency, Borgholm, Sweden, 1997.
- Hanson, D.R., and K. Mauersberger, Laboratory studies of the nitric acid trihydrate: implication for the south polar stratosphere, *Geophys. Res. Lett.*, **15**, 855-858, 1988.
- Hofmann, D. J., and T. Deshler, Stratospheric cloud observations during formation of the Antarctic ozone hole in 1989, *J. Geophys. Res.*, **96**, 2879-2912, 1991.
- Hofmann, D. J., T. Deshler, F. Arnold, and H. Schlager, Balloon observations of nitric acid aerosol formation in the Arctic stratosphere, 2, Aerosol, *Geophys. Res. Lett.*, **17**, 1279-1282, 1990.
- Hoppe, U.-P., G. Hansen, and D. Opsvik, Differential absorption lidar measurements of stratospheric ozone at ALOMAR: First results, *ESA SP-370*, pp. 335-344, Eur. Space Agency, 1995.
- Iraci, L. T., A. M. Middlebrook, M. A. Wilson, and M. A. Tolbert, Growth of nitric acid hydrates on thin sulfuric acid films, *Geophys. Res. Lett.*, **21**, 867-870, 1994.
- Iraci, L. T., A. M. Middlebrook, and M. A. Tolbert, Laboratory studies of the formation of polar stratospheric clouds: Nitric acid condensation on thin sulfuric acid films, *J. Geophys. Res.*, **100**, 20,969-20,977, 1995.
- Iraci, L. T., T. J. Fortin, and M. A. Tolbert, Dissolution of sulfuric acid tetrahydrate at low temperatures and subsequent growth of nitric acid trihydrate, *J. Geophys. Res.*, **103**, 8491-8498, 1998.
- Koop, T. U. M. Biermann, W. Raber, B. P. Luo, P. J. Crutzen, and Th. Peter, Do stratospheric aerosol droplets freeze above the ice frost point?, *Geophys. Res. Lett.*, **22**, 917-920, 1995.
- Koop, T., B. P. Luo, U. M. Biermann, P. J. Crutzen, and T. Peter, Freezing of  $\text{HNO}_3/\text{H}_2\text{SO}_4/\text{H}_2\text{O}$  solutions at stratospheric temperatures: Nucleation statistics and experiments, *J. Phys. Chem. A*, **101**, 1117-1133, 1997a.
- Koop T., K. S. Carslaw and Th. Peter, Thermodynamic stability and phase transitions of PSC particles, *Geophys. Res. Lett.*, **24**, 2199-2202, 1997b.
- Larsen, N., B. Knudsen, J.M. Rosen, N.T. Kjome, and E. Kyrö, Balloonborne backscatter observations of type I PSC formation: Inference about physical state from trajectory analysis, *Geophys. Res. Lett.*, **23**, 1091-1094, 1996.
- Luo, B., U. K., Krieger, and T. Peter, Densities and refractive indices of  $\text{H}_2\text{SO}_4/\text{HNO}_3/\text{H}_2\text{O}$  solutions to stratospheric temperatures, *Geophys. Res. Lett.*, **23**, 3707-3710, 1996.
- MacKenzie, A. R., A. Laaksonen, E. Batris, and M. Kulmala, The Turnbull correlation and the freezing of stratospheric aerosol droplets, *J. Geophys. Res.*, **103**, 10,875-10,884, 1998.
- Marti, J., and K. Mauersberger, Laboratory simulations of PSC particle formation, *Geophys. Res. Lett.*, **20**, 359-362, 1993.
- Mehrtens, H., U. von Zahn, F. Fierli, B. Nardi, and T. Deshler, Type I PSC-particle properties: Measurements at ALOMAR 1995 to 1997, *Geophys. Res. Lett.*, **26**, 603-606, 1999.
- Meilinger, S. K., T. Koop, B. P. Luo, T. Huthwelker, K. S. Carslaw, U. Krieger, P. J. Crutzen, and Th. Peter, Size-dependent stratospheric droplet composition in leewave temperature fluctuations and their potential role in PSC freezing, *Geophys. Res. Lett.*, **22**, 3031-3034, 1995.
- Middlebrook, A. M., L. T. Iraci, L. S. McNeill, B. G. Koehler, M. A. Wilson, O. W. Saastad, and M. A. Tolbert, Fourier transform-infrared studies of thin  $\text{H}_2\text{SO}_4/\text{H}_2\text{O}$  films: Formation, water uptake, and solid-liquid phase changes, *J. Geophys. Res.*, **98**, 20,473-20,481, 1993.
- Middlebrook, A.M., B. S. Berland, S. M. George, M. A. Tolbert, and O. B. Toon, Real refractive indices of infrared-characterized nitric-acid/ice films: Implications for optical measurements of polar stratospheric clouds, *J. Geophys. Res.*, **99**, 25,655-25,666, 1994.
- Mishchenko, M. I., L. D. Travis, and D. W. Mackowski, *T*-matrix computations of light scattering by nonspherical particles: A review, *J. Quant. Spectrosc. Radiat. Transfer*, **55**, 535-575, 1996.
- Molina, M. J., R. Zhang, P. J. Wooldridge, J. R. McMahon, J. E. Kim, H. Y. Chang, and K. D. Beyer, Physical chemistry of the  $\text{H}_2\text{SO}_4/\text{HNO}_3/\text{H}_2\text{O}$  system: Implications for polar stratospheric clouds, *Science*, **261**, 1418-1423, 1993.
- Poole, L. R., and M. P. McCormick, Airborne lidar observations of Arctic polar stratospheric clouds: Indications of two distinct growth stages, *Geophys. Res. Lett.*, **15**, 21-23, 1988.
- Pueschel, R. F., et al, Condensed nitrate, sulfate, and chloride in Antarctic stratospheric aerosols, *J. Geophys. Res.*, **94**, 11,271-11,284, 1989.
- Pueschel, R. F., K. G. Snetsinger, P. Hamill, J. Goodman, and M. P. McCormick, Nitric acid in polar stratospheric clouds: Similar temperature of nitric acid condensation and cloud formation, *Geophys. Res. Lett.*, **17**, 429-432, 1990.
- Ravishankara, A. R., and D. R. Hanson, Differences in the reactivity of Type I polar stratospheric clouds depending on their phase, *J. Geophys. Res.*, **101**, 3885-3890, 1996.
- Rosen, J. M., The vertical distribution of dust to 30 km, *J. Geophys. Res.*, **69**, 4673-4676, 1964.
- Rosen, J. M., N. T. Kjome, N. Larsen, B.M. Knudsen, E. Kyrö, R. Kivi, J. Karhu, R. Neuber, and I. Beninga, Stratospheric cloud threshold temperatures in the 1995-1996 arctic vortex, *J. Geophys. Res.*, **102**, 28195-28202, 1997.

- Schreiner, J., C. Voigt, A. Kohlmann, F. Arnold, K. Mauersberger, and N. Larsen, Chemical analysis of polar stratospheric cloud particles, *Science*, **283**, 968-970, 1999.
- Steele, H.M., and P. Hamill, Effect of temperature and humidity on the growth and optical properties of sulfuric acid-water droplets in the stratosphere, *J. Aerosol Sci.*, **12**, 517-528, 1981.
- Tabazadeh, A., R. P. Turco, and M. Z. Jacobson, A model for studying the composition and chemical effects of stratospheric aerosols, *J. Geophys. Res.*, **99**, 12,897-12,914, 1994.
- Tabazadeh, A., O. B. Toon, and P. Hammil, Freezing behavior of stratospheric sulfate aerosols inferred from trajectory studies, *Geophys. Res. Lett.*, **22**, 1725-1728, 1995.
- Tabazadeh, A., O. B. Toon, B. L. Gary, J. T. Bacmeister, and M. R. Schoeberl, Observational constraints on the formation of type Ia polar stratospheric clouds, *Geophys. Res. Lett.*, **23**, 2109-2112, 1996.
- Toon, O. B., O. B. Hamill, R. P. Turco, and J. Pinto, Condensation of HNO<sub>3</sub> and HCl in the winter polar stratospheres, *Geophys. Res. Lett.*, **13**, 1284-1287, 1986.
- Toon, O.B., E.V. Browell, S. Kinne, and J. Jordan, An analysis of lidar observations of polar stratospheric clouds, *Geophys. Res. Lett.*, **17**, 393-396, 1990.
- Vömel, H., M. Rummukainen, R. Kivi, J. Jarhu, T. Turunen, E. Kyrö, J. Rosen, N. Kjome, and S. Oltmans, Dehydration and sedimentation of ice particles in the Arctic stratospheric vortex, *Geophys. Res. Lett.*, **24**, 795-798, 1997.
- Worsnop, D. R., L. E. Fox, M. S. Zahniser, and S. C. Wofsy, Vapor pressures of solid hydrates of nitric acid: Implications for polar stratospheric clouds, *Science*, **259**, 71-74, 1993.
- Young, A.T., Revised depolarization correction for atmospheric extinction, *Appl. Opt.*, **19**, 3427-3428, 1980.
- Zhang, R., P. J. Wooldridge, J. P. D. Abbatt, and M. J. Molina, Physical chemistry of the H<sub>2</sub>SO<sub>4</sub>/H<sub>2</sub>O binary system at low temperatures: Stratospheric implications, *J. Phys. Chem.*, **97**, 7351-7358, 1993.
- Zhang, R., M. Leu, and M. J. Molina, Formation of polar stratospheric clouds on preactivated background aerosols, *Geophys. Res. Lett.*, **23**, 1669-1672, 1996.
- 
- A. Adriani, F. Cairo, and L. Pulvirenti, CNR-IFA, Via del Fosso del Cavaliere, 100 00133 - Roma, Italy. (adriani@atmos.ifa.rm.cnr.it; cairo@atmos.ifa.rm.cnr.it; pulvirenti@atmos.ifa.rm.cnr.it)
- T. Deshler and B. Nardi, Department of Atmospheric Science, University of Wyoming, P. O. Box 3038, Laramie, WY 82071. (deshler@uwyo.edu; nardi@ucar.edu)
- F. Fierli and A. Hauchercorne, Service d'Aeronomie du CNRS, BP 3 91371, Verrieres-Le-Buisson cedex, France. (fierli@aerov.jussieu.fr; hauchercorne@aerov.jussieu.fr)
- G. Hansen, Norwegian Institute for Air Research, NILU, The Polar Environmental Centre, N-9296 Tromsø, Norway. (georg@nilu.no)

(Received March 17, 1999; revised June 21, 1999; accepted June 23, 1999.)